Theoretical analysis and concept demonstration of a novel MOEMS accelerometer based on Raman–Nath diffraction

Zhang Zuwei(张祖伟)[1, 2, 3, †], Wen Zhiyu(温志渝)[1, 2, 3], and Hu Jing(胡晶)[1, 2, 3]

[1]Key Laboratory of Fundamental Science on Micro/Nano-Device and System Technology, Chongqing University, Chongqing 400030, China
[2]National Center for International Research of Micro/Nano-System and New Material Technology, Chongqing University, Chongqing 400030, China
[3]Microsystem Research Center of Chongqing University, Chongqing 400030, China

Abstract: The design and simulation of a novel microoptoelectromechanical system (MOEMS) accelerometer based on Raman–Nath diffraction are presented. The device is planned to be fabricated by microelectromechanical system technology and has a different sensing principle than the other reported MOEMS accelerometers. The fundamental theories and principles of the device are discussed in detail, a 3D finite element simulation of the flexural plate wave delay line oscillator is provided, and the operation frequency around 40 MHz is calculated. Finally, a lecture experiment is performed to demonstrate the feasibility of the device. This novel accelerometer is proposed to have the advantages of high sensitivity and anti-radiation, and has great potential for various applications.

Key words: accelerometer; MOEMS; Raman–Nath diffraction; FPW delay line oscillator
DOI: 10.1088/1674-4926/33/4/044005 **EEACC:** 2570

1. Introduction

Microelectromechanical system (MEMS) accelerometers are one of the most successful MEMS sensors. They have been intensively investigated and widely used in navigation, attitude control, air-bag systems, and so on. The operation of MEMS accelerometers is typically based on the displacement measurement of a proof mass suspended by elastic beams or thin diaphragms. The displacement of the proof mass can be measured by detecting the deflection directly or detecting the stress of the suspender beams or thin diaphragms. Most of today's MEMS accelerometers are based on capacitive and piezoelectric principles[1−8], and are not competent for working in hazardous atmospheres or in the presence of strong electromagnetic fields.

Recently, there have been some demonstrations of microoptoelectromechanical system (MOEMS) accelerometers. In common with MEMS accelerometers, MOEMS accelerometers generally detect the proof mass deflection or the stress generated by the proof mass. They have some advantages over MEMS accelerometers, including immunity to electromagnetic interference, remote sensing, high sensitivity and multiplexing ability. State-of-the-art MOEMS accelerometers can be divided into intensity-based, wavelength-encoded and interferometer-based modulation. The intensity-based MOEMS accelerometers are easy to set up, reliable and are low cost, but they have the drawback of sensitivity to external disturbances[9−12]. Wavelength-encoded MOEMS accelerometers usually use fiber Bragg grating as the wavelength modulator. They are not directly affected by external optical intensity change, but demand complex signal demodulation systems[13−16]. Interferometer-based MOEMS accelerometers are mainly based on Mach–Zehnder, Michelson, and Fabry–Perot configurations, and they provide the highest sensitivity in vibration sensing[17−21].

In this paper, a novel MOEMS accelerometer based on Raman–Nath diffraction is presented. Its operation principle is quite different from the reported MOEMS accelerometers, and it is proposed to be highly sensitive and immune to electromagnetic fields. The device will be fabricated by MEMS technology and consist of a flexural plate wave (FPW) delay line oscillator and optic strip waveguides. The FPW delay line oscillator works as an acousto-optic frequency shifter (AO shifter). When the light propagating in the optic strip waveguides passes through the AO shifter, Raman–Nath diffraction takes place. The sensing principle of the device is discussed in detail, the 3D finite element simulation of the FPW delay line oscillator is given out, and a lecture experiment is presented to demonstrate the principle of the MOEMS accelerometer.

2. Principle

The novel accelerometer mainly consists of an FPW delay line oscillator and optic strip waveguides. When an FPW delay line oscillator produces an acoustic wave propagating in a medium, the stress creates an optical index periodic variation. The variation functions as a diffraction grating. Either the Raman–Nath or the Bragg diffraction takes place when the light beam in the waveguide passes through the acoustic field. A criterion for distinguishing the two interaction regimes is defined by the Klein–Cook parameter Q[22]:

$$Q = 2\pi\lambda w/\lambda_{\rm a}^2 n, \tag{1}$$

where λ and $\lambda_{\rm a}$ are the wavelength of incident light and acoustic wave, respectively, n is the reflection index of the medium, and w is the effective width of the acoustic beam. Raman–Nath

† Corresponding author. Email: zhangzuwei00@163.com
Received 22 September 2011, revised manuscript received 12 December 2011 © 2012 Chinese Institute of Electronics

diffraction occurs when $Q < 1$, while Bragg diffraction occurs when $Q > 7$. The proposed accelerometer in this paper is based on Raman–Nath diffraction, so this is discussed in more detail below.

For Raman–Nath diffraction, the electric field of the mth order diffraction light can be expressed as:

$$B_m = A_m \cos(2\pi f t + 2\pi m f_a t + \phi_m), \tag{2}$$

while $B = A\cos(2\pi f + \phi)$ is the electric field of the incident light, where A and A_m are the amplitude of the incident light and the mth order diffraction light, respectively, ϕ and ϕ_m are the phase of the incident light and the mth order diffraction light, respectively, f is the frequency of incident light, f_a is the frequency of acoustic wave, and $m(= 0, \pm 1, \pm 2 \cdots)$ is the diffraction order. The successive diffraction light beams are separated by the diffraction angle, which is given by [22]:

$$\theta = \sin^{-1}\left(m\frac{\lambda}{\lambda_a}\right). \tag{3}$$

Assuming that the $+k$th and $-k$th order diffraction light beams are collected by receiving waveguides and then superimposed on an avalanche photodiode (APD), which is a square-law device in terms of electric field. The output current of the APD will be obtained as follows:

$$\begin{aligned} I &= \alpha\left[A_k \cos(2\pi f t + 2\pi k f_a t + \phi_k)\right. \\ &\quad \left.+ A_k \cos(2\pi f t - 2\pi k f_a t + \phi_{-k})\right]^2 \\ &= \alpha\left\{\frac{A_k^2}{2}\cos 2(2\pi f t + 2\pi k f_a t + \phi_k)\right. \\ &\quad + \frac{A_k^2}{2}\cos 2(2\pi f t - 2\pi k f_a t + \phi_{-k}) \\ &\quad - A_k^2 + A_k^2 \cos 2\left[2\pi f t + (\varphi_k - \varphi_{-k})/2\right] \\ &\quad \left.+ A_k^2 \cos 2\left[2\pi k f_a t + (\varphi_k - \varphi_{-k})/2\right]\right\}, \end{aligned} \tag{4}$$

where α is a constant respect to the APD. Because the response frequency of the APD is much lower than f but much higher than f_a, the output current I will be the superimposition of four DC components and one AC component, whose frequency is $2kf_a$. By detecting the APD output current, the acoustic wave frequency information can be obtained and amplified.

Because of the elastic thin plate structure and dispersive property of FPW, the resonant frequency of the FPW delay line oscillator will vary with the external acceleration, and it can be expressed as[23]:

$$f_N = \frac{1}{2\pi}\sqrt{\frac{1}{M}\left[D(N\pi/L)^4 + T(N\pi/L)^2\right]}, \tag{5}$$

where N is the acoustic wave mode order, D is the effective rigidity, L is the length of the plate, M is the mass per length, and T is the tension in the plate length direction. The change in external acceleration will result in a change in the plate length L, the tension T and the FPW resonant frequency f_a. Associated with the Raman–Nath diffraction discussed above, the acceleration change induced frequency information will be amplified by $2k$ times. In other words, the sensitivity of the accelerometer will be enhanced by $2k$ times, where k is the selected diffraction order.

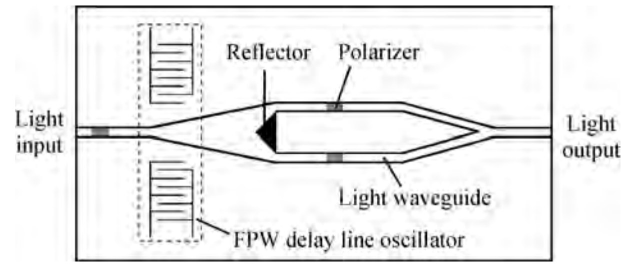

Fig. 1. Schematic of the accelerometer.

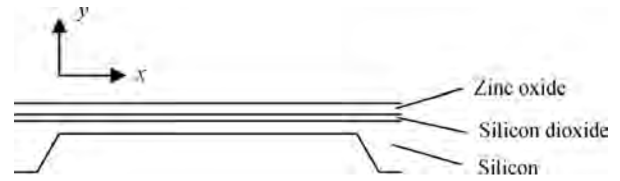

Fig. 2. Approximated beam structure of the FPW delay line oscillator.

Figure 1 shows a schematic of the novel MOEMS accelerometer. The device will be fabricated by MEMS technology. Firstly, three silicon dioxide layers are deposited on the silicon wafer to form the strip waveguides. The different refractive indexes of the three silicon dioxide layers are obtained by fine tuning the process parameters. Then the zinc oxide layer and the inter-digital electrodes are fabricated in the back etched membrane area, which is shown as the dashed box in Fig. 1, to form the FPW delay line oscillator. When a laser beam is coupled into and propagates along the waveguide, it interacts with the acoustic wave and diffracts in the Raman–Nath regime. Take the ± 5th order diffraction light beams for example, they are collected by two receiving waveguides, while the beams of lower order (0, ± 1st, $\cdots$, ± 4th order) are reflected by the aluminum reflector. There are three aluminum thin film polarizers on the surface of the waveguide to make sure the light beams have the same polarization. The collected ± 5th order diffraction light beams are guided together, superimposed and outputted to an APD, and the frequency of the APD output current is taken as the output of the accelerometer. If the external accelerometer induced frequency change of the FPW delay line oscillator is Δf_a, the output of the accelerometer will be $10\Delta f_a$. The sensitivity of the accelerometer is greatly improved by using Raman–Nath diffraction.

3. Simulation

As the key part of the accelerometer, the FPW delay line oscillator senses the change in external acceleration, as well as producing the acoustic field for Raman–Nath diffraction. The resonance frequency of the FPW delay line oscillator is very important and must be predicted. So the theoretical analysis and finite element simulation are adopted to calculate the resonance frequency of the FPW delay line oscillator.

The FPW delay line oscillator can be approximated as a multilayered thin plate structure built-in at both ends, as shown in Fig. 2. The thin plate consists of zinc oxide, silicon dioxide and silicon, whose characteristics are summarized in Table 1. Weinberg *et al.* gave the FPW resonant frequency of different

Table 1. Parameters of the multilayered beam.

Layer	Length (μm)	Width (μm)	Thickness (μm)	Mass density (g/cm^3)	Modulus (GPa)	Poisson's ratio
Zinc oxide	3600	700	3	5.680	120	0.33
Silicon dioxide	3600	700	2	2.200	70	0.17
Silicon	3600	700	15	2.239	170	0.28

modes with external force in the x direction, which is shown as Eq. (5). In the expression, D is an effective rigidity for the multilayer structure, which can be given by[23]:

$$D = \sum_i \frac{E_i \left(I_i + S_i Y_i^2\right)}{1 - \nu_i^2}, \tag{6}$$

in which, $Y_i = y_i - y_{\rm M}$ and $y_{\rm M} = \sum\limits_i \frac{y_i E_i S_i}{1-\nu_i^2} / \sum\limits_i \frac{E_i S_i}{1-\nu_i^2}$, where i is the index for a material layer, E is Young's modulus, S is the layer cross-section area, y is the vertical distance from the center of the area to an arbitrary reference, ν is Poisson's ratio, and I is the area moment of inertia for each layer calculated about its center of area. When external acceleration is not applied and the thermal expansion is ignored, the parameter T can be considered as zero. The wavelength of the FPW is the period of the interdigital electrodes (IDT), which is 80 μm. Substitute Eq. (6) into Eq. (5), and the fundamental resonant frequency of the FPW delay line oscillator can be theoretically calculated as 41.1 MHz.

When external acceleration is applied, the maximum strain and stress in the x direction at the top surface of the plate can be expressed as[24]:

$$\varepsilon = \frac{3LM_{\rm ass}a}{4DWH^2}, \tag{7}$$

$$\sigma = D\varepsilon, \tag{8}$$

where ε is the strain, $M_{\rm ass}$ is the proof mass, a is the external acceleration, W is the width of the plate, H is the thickness of the plate, and σ is the stress. Actually, the strain and the stress distributions on the plate are not uniform. In order to simplify the analysis and calculation of the frequency sensitivity of the FPW delay line oscillator to the external acceleration, ε and σ are considered as the average strain and stress of the plate roughly. The plate length will change to:

$$L' = L(1 - \varepsilon), \tag{9}$$

and the tension T can be given by:

$$T = \sigma WH. \tag{10}$$

Substitute Eqs. (6), (9) and (10) into Eq. (5), and assume that a silicon proof mass with a size of 5 × 5 × 0.2 mm^3 is connected to the plate, the relationship between the FPW delay line oscillator frequency and the acceleration is obtained as in Fig. 3. The sensitivity of the FPW delay line oscillator to the acceleration can be roughly calculated as 130 kHz/g. If the ±2nd order diffraction beams are utilized, the sensitivity of the proposed accelerometer will be 520 kHz/g.

A 3D finite element mode of the FPW delay line oscillator is created by ANSYS, as shown in Fig. 4. The harmonic response analysis and transient analysis are performed subsequently.

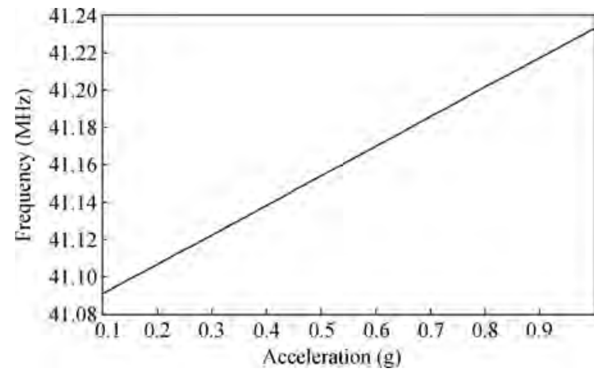

Fig. 3. Relationship between the FPW delay line oscillator frequency and acceleration.

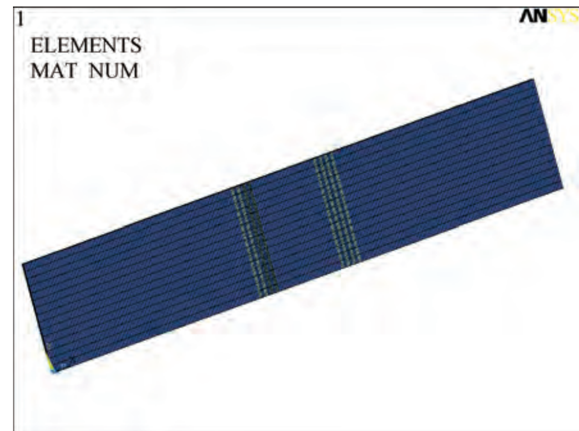

Fig. 4. 3D finite element mode of the FPW delay line oscillator.

Firstly, a sine sweep voltage (0–55 MHz) is applied to the IDT, and the harmonic response analysis is used to calculate the strain response of the thin plate to the voltage at different frequencies. Figure 5 is the strain response curve versus frequencies, and there are two response peaks at 20.4 and 37.2 MHz, respectively, corresponding to the resonant frequencies of the acoustic waves propagating in the thin plate. The vibration modes at the two resonant frequencies are presented in Figs. 6 and 7, respectively. It can be seen that the vibration at 37.2 MHz is the expected anti-symmetric mode. By using harmonic response analysis, the fundamental resonant frequency of the anti-symmetric mode of the FPW is calculated as 37.2 MHz. The comparison of the harmonic analysis result with the theoretical result shows that the relative error of resonant frequency is 9.7%.

Then, a DC impulse is applied to the IDT, and transient analysis is used to calculate the vibration waveforms of the

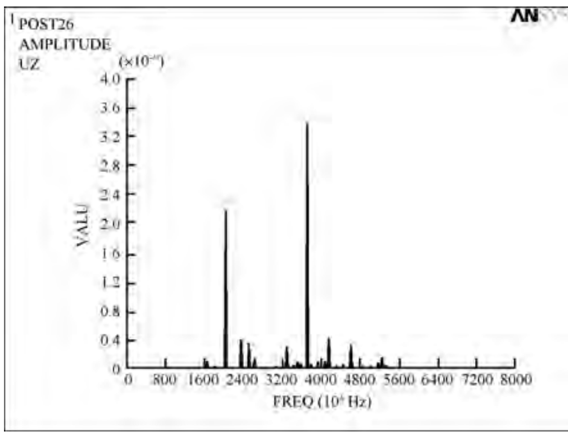

Fig. 5. Strain response at different frequencies obtained by harmonic analysis.

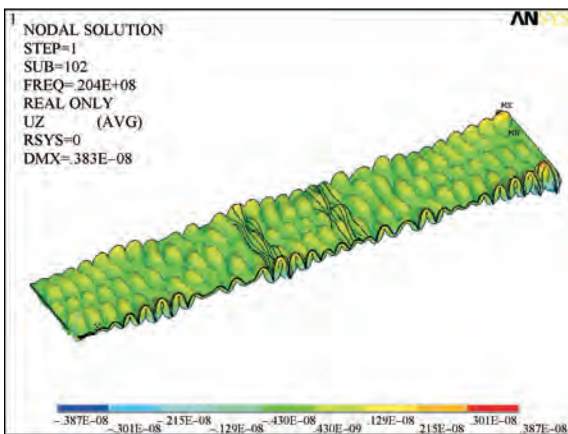

Fig. 6. Vibration modes at the frequency of 20.4 MHz.

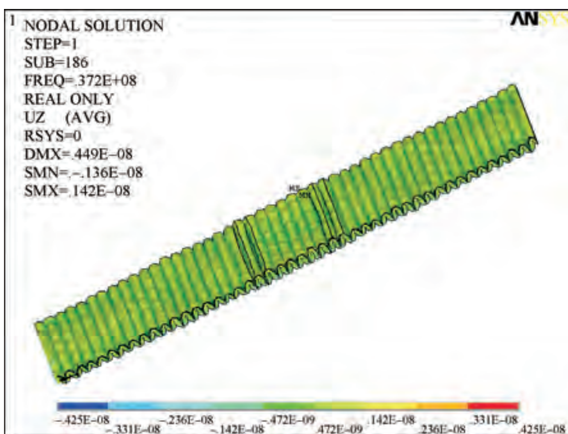

Fig. 7. Vibration modes at the frequency of 37.2 MHz.

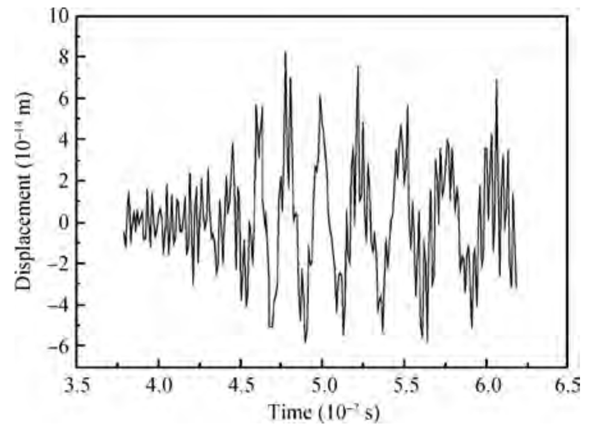

Fig. 8. Vibration waveform obtained by transient analysis.

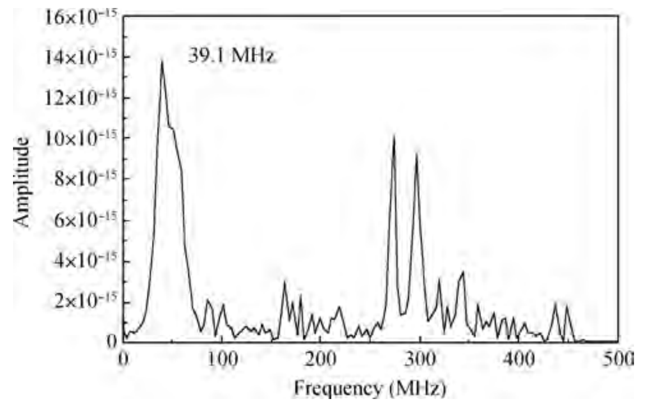

Fig. 9. Fourier transform pattern of the vibration waveform obtained by transient analysis.

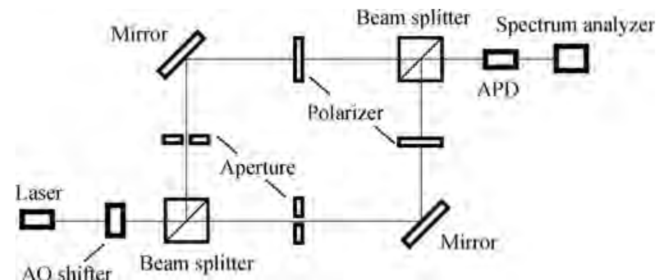

Fig. 10. Schematic diagram of the macro model of the accelerometer.

particles in the thin plate. The vibration performs a sinusoidal format as shown in Fig. 8. The Fourier transform pattern of the vibration waveform, as shown in Fig. 9, shows the dominating frequency of 39.1 MHz, which indicates that the fundamental resonant frequency of the anti-symmetric mode of the FPW is 39.1 MHz. A comparison of the transient analysis result with the theoretical result shows that the relative error of resonant frequency is 5.3%.

4. Concept demonstration

A macro model was established and a lecture experiment was presented to demonstrate the feasibility of the accelerometer. A schematic diagram is shown in Fig. 10, and a picture of the experimental system is shown in Fig. 11. The incidence laser beam passes through an AO shifter whose operating frequency is 15 MHz, and Raman–Nath diffraction takes place. The diffraction light beams are divided into two parts by a beam splitter, the reflected beams and the transmitted beams. The reflected beams are incident on an aperture and only the $+1$st order diffraction beam is allowed to pass through, while only the -1st order diffraction beam of the transmitted beams is allowed to pass through. Propagating through the polarizer, the

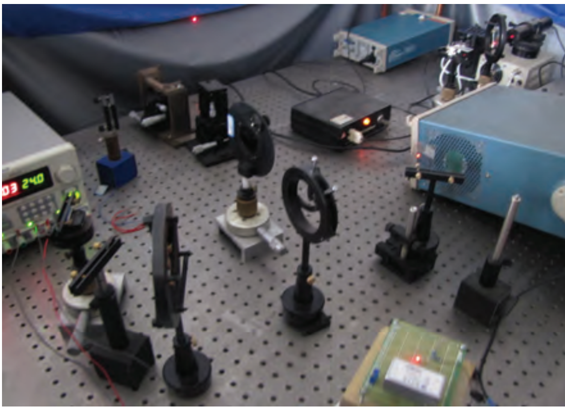

Fig. 11. Picture of the experimental system.

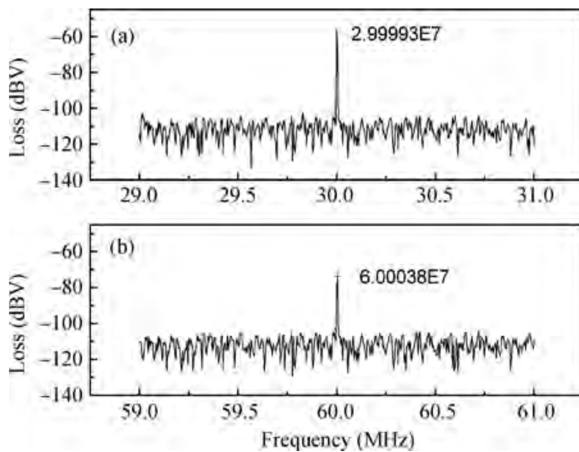

Fig. 12. Output electric signal of the APD when (a) the $\pm$1st diffraction beams and (b) the $\pm$2nd diffraction beams are utilized, respectively.

$+$1st order and –1st order diffraction beams with the same polarization are superimposed and incident on an APD (AD500-8 TO52S2). The output electric signal of the APD is displayed by a spectrum analyzer. The AO shifter is operated at 15 MHz, and the output signal of the spectrum analyzer is shown as in Fig. 12. Figures (a) and (b) represent the output signals when the $\pm$1st and the $\pm$2nd order diffraction beams are utilized, respectively. It can be seen that when the acoustic wave frequency is 15 MHz, a 30 MHz electric signal can be obtained using the $\pm$1st order diffraction beams, while a 60 MHz electric signal can be obtained using the $\pm$2nd order diffraction beams. That is to say, if the acceleration induces an acoustic frequency change of Δf_a, an electric frequency of $2n\Delta f_a$ will be obtained by using the $+n$th order and $-n$th order diffraction beams. The principle of the novel accelerometer is therefore approved.

5. Conclusion

The MOEMS accelerometer is an important MEMS accelerometer research branch with great potential. In this paper, the theoretical analysis and concept demonstration of a novel MOEMS accelerometer based on Raman–Nath diffraction is given out. The device mainly consists of an FPW delay line oscillator and optic strip waveguides, and will be fabricated by MEMS technology. Firstly, the sensing principle of the device is discussed carefully. Then, a 3D finite element mode of the FPW delay line oscillator is created by ANSYS, the harmonic response analysis and transient analysis are taken out, and the fundamental resonance frequency of the FPW delay line oscillator is calculated around 40 MHz. Finally, a macro model is established and the principle of the accelerometer is demonstrated by a lecture experiment. The fabrication of the device is now ongoing, and this, along with the testing of the device, will be discussed in the next paper. This novel MOEMS accelerometer is proposed to have the advantages of high sensitivity and anti-radiation, and should have great potential in various applications.

References

[1] DeVoe D L, Pisano A P. A fully surface-micromachined piezoelectric accelerometer. International Conference on Solid State Sensors and Actuators, 1997: 1205

[2] Chau K H L, Lewis S R, Zhao Y, et al. An integrated forced-balanced capacitive accelerometer for low-g applications. Sens Actuators A: Phys, 1996, 54: 472

[3] Tsai M, Liu Y, Sun C, et al. A CMOS-MEMS accelerometer with tri-axis sensing electrodes arrays. Procedia Eng, 2010, 5: 1083

[4] Liu S, Ma T, Hou W. Design and fabrication of a new miniaturized capacitive accelerometer. Sens Actuators A: Phys, 2008, 47: 70

[5] Sun C, Wang C, Fang W. On the sensitivity improvement of CMOS capacitive accelerometer. Sens Actuators A: Phys, 2008, 141: 347

[6] Wen L, Haspeslagh L, De Coster J, et al. Design and characterization of a CMOS compatible poly-SiGe low g capacitive accelerometer. Procedia Eng, 2010, 5: 742

[7] Kanda K, Iga Y, Matsuoka J, et al. A tri-axial accelerometer with structure-based voltage operation by using series-connected piezoelectric elements. Procedia Eng, 2010, 5: 894

[8] Dong P, Li X, Yang H, et al. High-performance monolithic triaxial piezoresistive shock accelerometers. Sens Actuators A: Phys, 2008, 141: 339

[9] Kalenik J, Pajak R. A cantilever optical-fiber accelerometer. Sens Actuators A: Phys, 1998, 68: 350

[10] Plaza J A, Llobera A, Dominguez C, et al. BESOI-based integrated optical silicon accelerometer. J Microelectromech Syst, 2004, 13: 355

[11] De Doncker H W J A, Guan T, Driesen M, et al. Biaxial and uniaxial epoxy accelerometers. Procedia Chemistry, 2009, 1: 572

[12] Cadarso V J, Llobera A, Villanueva G, et al. Polymer microoptoelectromechanical systems accelerometers and variable optical attenuators. Sens Actuators A: Phys, 2008, 145/146: 147

[13] Storgaard-Larsen T, Bouwstra S, Leistiko O. Opto-mechanical accelerometer based onstrain sensing by a Bragg grating in a planarwaveguide. Sens Actuators A: Phys, 1996, 52: 25

[14] Shi C Z, Zeng N, Hu H L, et al. Cantilever optical vibrometer using fiber Bragg grating. Opt Eng, 2003, 42: 3179

[15] Fender A, Macpherson W N, Maier R R J, et al. Two-axis temperature insensitive accelerometer based on multicore fiber Bragg gratings. IEEE Sensors Journal, 2008, 8: 1292

[16] Zhou W, Dong X, Ni K, et al. Temperature-insensitive accelerometer based on a strain-chirped FBG. Sens Actuators A: Phys, 2010, 157: 15

[17] Wu B, Chen C, Ding G, et al. Hybrid-integrated Michelson fiber

optic accelerometer. Opt Eng, 2004, 43: 313

[18] Perez M, Eklund E J, Shkel A M. Designing micromachined accelerometers with interferometric detection. IEEE Sens, 2005: 652

[19] Ke T, Zhu T, Rao Y, et al. Accelerometer based on all-fiber Fabry–Perot interferometer formed by hollow-core photonic crystal fiber. Microw Opt Technol Lett, 2010, 52: 2531

[20] Nayak J, Srinivas T, Selvarajan A, et al. Design and analysis of micro-opto-electro-mechanical accelerometer. Proc SPIE, 2003, 5062: 773

[21] Gangopadhyay T K. Prospects for fiber Bragg gratings and Fabry–Perot interferometers in fiber-optic vibration sensing. Sens Actuators A: Phys, 2004, 113: 20

[22] Wu Y, Shankar P M, Lewin P A, et al. Fiber optic ultrasonic sensor using Raman–Nath light diffraction. EEE Trans Ultrasonics Ferroelectrics, and Frequency Control, 1994, 41: 166

[23] Weinlerg M S, Cunningham B T, Clapp C W. Modeling flexural plate wave devices. J Microelectromchan Syst, 2000, 9: 370

[24] Wang Z. Microsystem design and fabrication. Beijing: Tsinghua University Press, 2008